Concentration and potential distributions in the active layer of proton exchange membrane fuel cell electrodes[†]

Y. BULTEL, P. OZIL and R. DURAND
Laboratoire d'Electrochimie et de Physico-chimie des Matériaux et des Interfaces, U.M.R. INPG-CNRS 5631 associated to UJF, ENSEEG, BP 75, 38402 St Martin d'Hères, France

Abstract

This work is focussed on modelling mass and charge transfer limitations within an active layer considering uniform distribution of catalyst phase (classical model) or a more realistic discrete distribution (modified model). A model is proposed here based on soft-coupled equations describing diffusion, ionic ohmic drop and interfacial charge. It is applied to the practical case of oxygen reduction or hydrogen oxidation for PEM fuel cells. Simulation shows that the modified model has to be used for fast kinetics, that is, when the local limitations become predominant. In contrast, the classical flooded homogeneous model remains suitable when mass and charge transport resistances are negligible at the particle level.

List of symbols

a interparticle distance (m)
b Tafel slope (V decade^{-1})
C concentration (mol m^{-3})
d mean particle diameter (m)
D diffusion coefficient (m^2 s^{-1})
F faradaic constant (96 500 C mol^{-1})
i current density (A m^{-2})
i_o exchange current density per real catalyst area (A m^{-2})
L active layer thickness (m)
n total number of electrons involved in the electrochemical reaction
n   normal vector
R gas constant (8.31 J K^{-1} mol^{-1})
T temperature (K)
U, u dimensionless parameters (–)
V, v dimensionless parameters (–)
z abscissa (m)

Greek symbols
α_e transfer coefficient
ε effectiveness factor (–)
Φ potential (V)
γ real catalyst area/geometric area ratio (m^2 m^{-2})
η local overpotential (V)
φ flux density (mol m^{-2} s^{-1})
κ ionic conductivity within the L electrolyte phase (S m^{-1})
Π reduced overpotential (–)
Γ reduced concentration (–)

Subscript
o   index referring to the gas–electrolyte interface

1. Introduction

Many models have been developed to describe the working behaviour of PEM fuel cell (PEMFC) active layers. For PEMFC, three types of model are usually considered: the homogeneous flooded, the thin film and agglomerate models [1–3]. These models are used to simulate the working behaviour of fuel cell electrodes [4–8]. They also allow estimation of the kinetic parameters (exchange current density, Tafel slope) of the electrochemical reactions occurring in their active layers. In this latter case, the experimental results obtained with a rotating disc electrode [9, 10] or a gas diffusion electrode [11] can be corrected for mass and charge transport limitations by using classical [9, 10] or modified [12, 13] models depending on the working conditions.

The classical models all consider a catalyst phase evenly distributed and intimately mixed with the electrolyte. As a result the predicted performances of the fuel cell can only take into account the transport limitations at the scale of the whole active layer. Nevertheless, previous studies showed that unexpected diffusion [14, 16] and ohmic drop [15] effects occur at the particle level so decreasing performances. These latter effects were obtained by considering a more realistic

---

[†] Dedicated to the memory of Daniel Simonsson

discrete distribution of catalyst phase as isolated nano-particles flooded in electrolyte.

The present work is focused on the influence of the discrete distribution of the catalyst phase on the electrode performance. The comparison between the models demonstrates that the classical model dramatically overestimates the kinetic current densities for high current densities. This unexpected effect is then investigated, calculating concentration and overpotential distributions for a thin active layer without gas pores. Simulations from a modified model taking into account the local effects are presented for oxygen reduction at the cathode and hydrogen oxidation at the anode. These are compared to predictions provided by classical models and show a deviation from the linear profile concentration and overpotential close to the catalyst particles. Finally, some dimensionless criteria U, u, V, v, d/a are proposed to characterize the mass or charge transfers at the whole active layer and at the particle level. These allow identification of limiting mechanisms in the active layer and confirmation of the appropriate model to describe its behaviour. Parameters U and u are similar to modified Damköhler numbers, they quantify the influence of diffusion mass transport compared to kinetics at the level of either the active layer (U) or the particles (u). Similarly, parameters V and v are reciprocals of modified Wagner numbers defined as the ratios of the electrolyte ohmic resistance to the resistance to charge transfer at the electrode. The dimensionless ratio d/a highlights the competitive effect between neighbouring particles. However, this effect is negligible [14–16] and is not studied here.

2. Active layer modelling

2.1. Description of a nonporous active layer

The active layer of a PEM fuel cell consists of a solid polymer electrolyte (usually Nafion®), PTFE and electrocatalyst nanoparticles, generally platinum deposited on carbon grain. The gas species, hydrogen at the anode and oxygen at the cathode, are dissolved at the gas–electrolyte interface and diffuse toward nanoparticles where they react by anodic oxidation or cathodic reduction. Diffusion can be described by Fick's law (Equation 1), conduction by Ohm's law (Equation 2)

$$\varphi = -D|\text{grad}(C)| \tag{1}$$

$$i = -\kappa|\text{grad}(V)| \tag{2}$$

Far from equilibrium, the oxygen reduction mechanism involves a multistep reaction and is classically described by the Tafel equation [17]:

$$-i = i_o \left[\exp\left(\frac{-2.3\,\eta_c}{b_c}\right) \right] \frac{C_{\text{red}}}{C_{0,\text{red}}} \tag{3a}$$

For hydrogen oxidation and a for high current density corresponding to a low coverage rate, the Tafel equation provides a suitable approximate kinetic model by neglecting the reverse term:

$$i = i_o \left[\exp\left(\frac{2.3\,\eta_a}{b_a}\right) \right] \frac{C_{\text{ox}}}{C_{0,\text{ox}}} \tag{3b}$$

where b_c and b_a are the Tafel slopes.

For oxygen reduction on small platinum particles, the kinetic parameters are well known (Table 1) and strongly depend on the working temperature of the electrode which can vary between 298 and 353 K [17]. For hydrogen oxidation, however, the lack of accurate data prompted consideration of a wide range of values for the kinetic parameters as shown in Table 2. A Tafel slope of 0.03–0.04 V decade^{-1} has been proposed by Ticianelli et al. [18].

Recast Nafion® exhibits a strong dependence of ionic conductivity on temperature and water content. The product of diffusion coefficient, D, and solubility C_0 can vary from 10^{-9} to 4×10^{-9} mol m^{-1} s^{-1} for oxygen [17] and from 10^{-10} to 10^{-9} mol m^{-1} s^{-1} for hydrogen [18], when temperature ranges from 298 to 353 K. Moreover, ionic conductivity falls strongly with decreasing humidity or temperature. In practical conditions, ionic conductivity [19] can vary between 10^{-1} to 10 S m^{-1}.

2.2. Classical model

The classical flooded homogeneous model [10] is widely used to describe mass and charge transfer in a nonporous active layer. It considers that electrolyte and carbon grains supporting catalyst particles are two intimately mixed phases (Figure 1). As a consequence, the dissolved species (hydrogen or oxygen) simultaneously diffuse and react in the catalyst layer while protons migrate across the electrolyte (Figure 1). Moreover in the absence of gas pores, the dissolved species (oxygen or hydrogen) diffuse from the gas-active layer interface to the active layer-membrane interface while protons

Table 1. Variation ranges for the electrochemical parameters of oxygen reduction [17]

O$_2$	Exchange current i_o /A m^{-2}	Tafel slope b /V decade^{-1}	Total overpotential η_o /V
Low current density	10^{-6}–10^{-4}	0.060–0.070	$\eta_o < 0.40$
High current density	10^{-3}–10^{-2}	0.115–0.125	$\eta_o > 0.40$

Table 2. Variation ranges for the electrochemical parameters of hydrogen oxidation [18]

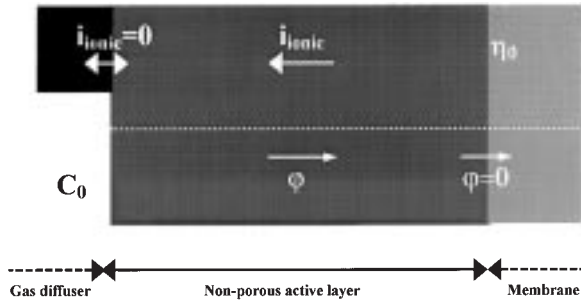|	Exchange current i_o /A m^{-2}	Tafel slope b /V decade^{-1}	Total overpotential η_o /V
H$_2$ anode	10^1–10^2	0.030–0.120	$\eta_o < 0.15$

Fig. 1. Classical homogeneous flooded model for an active layer without gas pores.

migrate from the membrane–active layer interface to the active layer–gas interface. So, this model assumes that diffusion and migration occur in opposite directions along the z axis while electronic ohmic drop is negligible compared to ionic drop.

For an isothermal system under steady state conditions, local mass and charge balances lead to the one-dimensional equations:

$$D\frac{\partial^2 C}{\partial z^2} - \frac{\gamma_L i_o}{nFL}\left[\exp\left(\frac{2.3|\eta|}{b}\right)\frac{C}{C_0}\right] = 0 \qquad (4)$$

$$\kappa\frac{\partial^2 \eta}{\partial z^2} - \frac{\gamma_L i_o}{L}\left[\exp\left(\frac{2.3|\eta|}{b}\right)\frac{C}{C_0}\right] = 0 \qquad (5)$$

These can be solved numerically in respect of the following boundary conditions.
(i)   At the gas–active layer interface, the concentration is equal to solubility and the ionic current density is zero:

$$z = 0, \quad C = C_0, \quad \kappa\vec{\nabla}|\eta| = \vec{0} \qquad (6)$$

(ii)   At the membrane–active layer interface, the total overpotential is constant and the mass flux density is zero:

$$z = L, \quad \eta = \eta_0, \quad D\vec{\nabla}C = \vec{0} \qquad (7)$$

A dimensionless formulation provides a more suitable description for studying mass and charge transfer within the active layer:

$$\frac{\partial^2 \Gamma}{\partial x^2} - U(\Pi)\Gamma = 0 \qquad (8)$$

with

$$U(\Pi) = \frac{\gamma_L i_k(\Pi)L}{nFDC_0}, \quad \Gamma = \frac{C}{C_0}$$

$$\frac{\partial^2 \Pi}{\partial x^2} - V(\Pi)\Gamma = 0 \qquad (9)$$

with

$$V = \frac{2.3\,\gamma i_k L}{\kappa b}, \quad \Pi = \frac{2.3\,\eta}{b}$$

The classical models highlight two dimensionless parameters U [15] and V [14] characterizing, respectively, the mass and charge transfer limitations at the level of the whole active layer thickness.

Neglecting ohmic drop limitation, the mass balance (Equation 4) leads to an analytical expression for the concentration against Z (= z/L). On the other hand, the charge balance (Equation 5), without diffusion limitation, leads to an equation that can be solved via a Newton–Raphson method [20]. In the most general case this method is also required to solve the mass and charge balance equations (Equations 8 and 9) when considering diffusion and ohmic drop limitations.

2.3. Modified model

We propose here a modified flooded model for a nonporous active layer in order to analyse the geometric effect due to the discrete distribution of catalyst. The main difference between the classical and modified models is that the catalyst particles are distributed following a hexagonal three-dimensional network of spherical particles within the electrolyte [11, 15] (Figure 2).

Using this distribution for every particle line, six symmetry planes can be considered around every particle and its neighbours. In such conditions, the hexagonal symmetry can be approximated by a cylindrical symmetry and the equations have to be rewritten in cylindrical coordinates (Figure 3). Simulations were performed by using the finite element method (commercial software Flux-Expert®) with axisymmetric equations and a two dimensional grid. This approach using the finite element method allows, not only to take into account the mass and charge transport at the particle
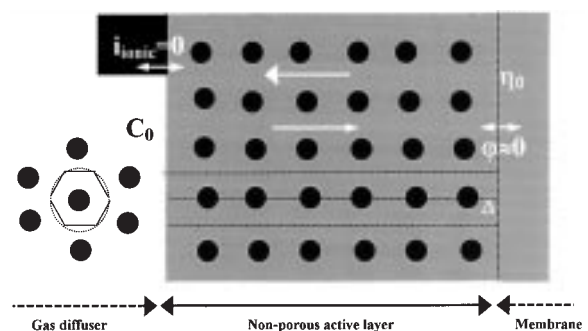

Fig. 2. Modified model considering the discrete distribution of catalyst phase as nanoparticles.
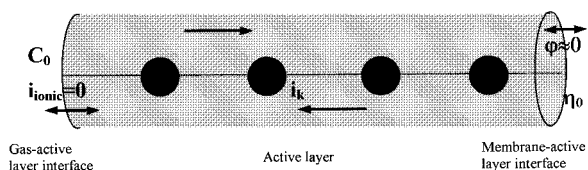

Fig. 3. Hexagonal 3D network of spherical particles. Modified model.

level, but also the competition effect between neighbouring particle, as suggested by Stonehart [21].

In the most general case, both diffusion and ionic ohmic drop in the electrolyte are considered and act in opposite direction for a nonporous active layer with an electrochemical Tafel law at the electrolyte–particle interface (Figure 3). This case is described by the soft coupled equations (Equations 10, 11 and 12) leading to a system of partial derivate equations to be solved with the same boundary conditions as for the classical model:

$$\nabla \cdot (D\nabla C) = 0 \tag{10}$$

$$\nabla \cdot (\kappa\nabla\eta) = 0 \tag{11}$$

$$i = i_{\mathrm{o}}\left[\exp\left(\frac{2.3\,\eta}{b}\right)\frac{C}{C_0}\right] \tag{12}$$

If diffusion is the rate determining step relative to ohmic drop, the potential remains fairly constant anywhere within the electrolyte and thus the Tafel equation can be

reduced to a single order kinetic law. Thus, the numerical formulation will be described using Equations 10 and 12: Fick's law and a single order kinetic equation with soft coupling at the particle interface [16]. It is completed by the boundary conditions: a Dirichlet condition at the gas-electrolyte interface ($C = C_0$) and homogeneous Neuman condition at the membrane–active layer interface ($\varphi = 0$).

If diffusion is negligible relative to ohmic drop, the concentration remains fairly constant. The numerical formulation then consists of writing the soft-coupled Ohm and Tafel equations (Equations 11 and 12) to describe charge transfer at the electrolyte–particle interface [15]. These equations have to be solved in the respect of the following boundary conditions: a Dirichlet condition at the membrane–active layer interface ($\eta = \eta_0$) and a homogeneous Neuman condition ($i = 0$).

Considering both diffusion and ionic ohmic drop limitation, the numerical formulation then consists of writing the soft-coupled diffusion, Ohm and Tafel laws (Equations 10, 11 and 12) to describe the charge transfer at the electrolyte–particle interface. These equations can be directly solved by the software Flux–Expert® through an iterative algorithm using the classical finite element method (see appendix).

2.4. Dimensionless formulation

In this case, the dimensional analysis highlights three extra parameters in addition to the dimensionless parameters defined for the classical model: the parameters u [14, 16], v [15] related to the transfer at the

Table 3. Dimensionless parameters of mass and charge transfer resistances

	Mass transfer resistance		Charge transfer resistance	
Referred to the active layer level ($\propto \gamma L$)	$U = \dfrac{\gamma i_{\mathrm{k}}L}{nF\,DC_0}$	(13)	$V = \dfrac{\gamma i_{\mathrm{k}}L}{\kappa b}$	(14)
Referred to the particle level ($\propto d/2$)	$u = \dfrac{i_{\mathrm{k}}(d/2)}{nF\,DC_0}$	(15)	$v = \dfrac{i_{\mathrm{k}}(d/2)}{\kappa b}$	(16)

catalyst particle (Table 3) and the dimensionless geometrical ratio d/a [14–16]. As a result, the dimensionless expression for the effectiveness factor ε is a function of only five independent parameters.

The effectiveness factor characterises the electrocatalyst utilization and is defined as the ratio of the experimental electrode current density to the kinetic electrode current density (without limitations due to ohmic drop and diffusion) [22]:

$$\varepsilon = \frac{\text{experimental current density}}{\text{kinetic current density (without mass and ohmic drop limitations)}} \tag{13}$$

Thus, the experimental current density referred to the geometrical area can be written as

$$i_{\exp} = \gamma\,\varepsilon\,i_{\mathrm{k}} \tag{14}$$

Under kinetic control, diffusion and ohmic drop resistances are negligible compared to charge transfer resistance ($U \ll 1$, $V \ll 1$) and the catalyst utilization rate ε remains close to unity. In contrast, for fast electrochemical reactions, mass and charge transport resistances are no longer negligible in the whole active layer level ($U \gg 1$, $V \gg 1$) and then the catalyst utilization rate decreases strongly. Moreover, at the particle level, mass and charge transport limitations become predominant when the dimensionless parameters u and v tend to unity. Then transport resistances cannot be neglected at the particle level and consequently the classical models are no longer suitable for describing the working behaviour of the active layer. Such conditions require use of the modified models [12, 13]. On the other hand, the classical model is appropriate when local parameters u and v are considerably less than unity.

Hence the dimensionless parameters defined for this study are useful for identifying the limiting steps. As a simplified rule, transport limitations are no longer negligible compared to kinetics when the dimensionless parameters are close to unity or greater.

3. Results and comments

Diffusion limitations are classically considered at the level of the whole active layer in gas diffusion electrodes

[10]. Nevertheless, ionic ohmic drops are not always insignificant compared to diffusion depending on overpotential, temperature, humidity and on the nature of the ionomer. Moreover, diffusion and migration effects at the particle level [15, 16] are not negligible relative to limitation at the whole active layer level. Therefore, it is important first to compare the polarization curves predicted by the classical models and the modified one. This study is performed here for a realistic weakly porous active layer ($L = 10$ μm and $\gamma = 32$ cm^2 cm^{-2}) by using the kinetic parameters for cathodic oxygen reduction and anodic hydrogen oxidation at the cathode presented respectively in Tables 1 and 2. Thus, the comparison of concentration and potential distributions predicted by both models, in the case of a very thin active layer without gas pores ($L = 1$ μm, $d = 10$ nm, $a = 100$ nm), gives unexpected results due to the contribution of the discrete distribution of the catalyst phase. This effect may be explain in term of mass transport and ohmic resistance at the particle level. Unfortunately, for a large active layer ($L \gg a$), it is impossible to present the concentration and potential profiles. Thus, a thinner active layer (active layer thickness about 1 μm particle diameter about 10 nm and interparticle distance about 0.1 μm) is used, which allows the concentration and potential profiles close to the catalyst particles to be calculated.

3.1. Cathodic oxygen reduction: case of slow kinetics

Figure 4 shows the polarisation curves obtained with the classical and modified flooded homogeneous models. When considering both diffusion and ohmic drop limitations, the predicted current densities are unchanged for potentials ranging from 300 to 700 mV. The discrete distribution of the catalyst phase seems to induce no effect for oxygen reduction.

If using a thinner active layer (Figure 5), the concentration steadily declines from the gas–electrolyte interface to the electrolyte–membrane interface while the potential is quite constant. This later expected result corresponds to dimensionless parameters V and v always smaller than unity due to slow kinetics and high ionic conductivity. Moreover, the dimensionless parameter u remains smaller than 1 and the concentration profiles maintain a quasi-linear shape. Consequently, ohmic drop resistance remains negligible and diffusion in the active layer is weakly modified by the discrete distribution of catalyst phase as isolated nanoparticles.

For oxygen reduction which is characterised by slow kinetics, parameters u and v referred to the diffusion and ionic ohmic drop at the particle level are always smaller than unity. As a result, the modified model predicts almost the same concentration profiles as the classical model (Figure 6) and, consequently, the expected real kinetic current density (or catalyst utilization rate) are identical (Figure 4) [14, 16]. Here a discrete distribution is of no interest in describing the catalyst phase because it does not improve the knowledge of the oxygen concentration and potential profiles. In such conditions, the classical model is suitable for prediction of the working behaviour of the cathode.

For a very thin active layer thickness, ohmic drop is negligible (V, $v \ll 1$). The concentration distribution predicted in the general case (Figure 5(a)) is weakly modified and is similar to those predicted when considering only diffusion (Figure 6(a)). However, for a larger and more realistic active layer, the predicted current densities are greater when considering only diffusion rather than both diffusion and ohmic drop limitation (Figure 4). In this case, the dimensionless parameter V increases while v remains constant and smaller than unity. Consequently, the ionic ohmic drop limitation can no longer be neglected over the whole active layer
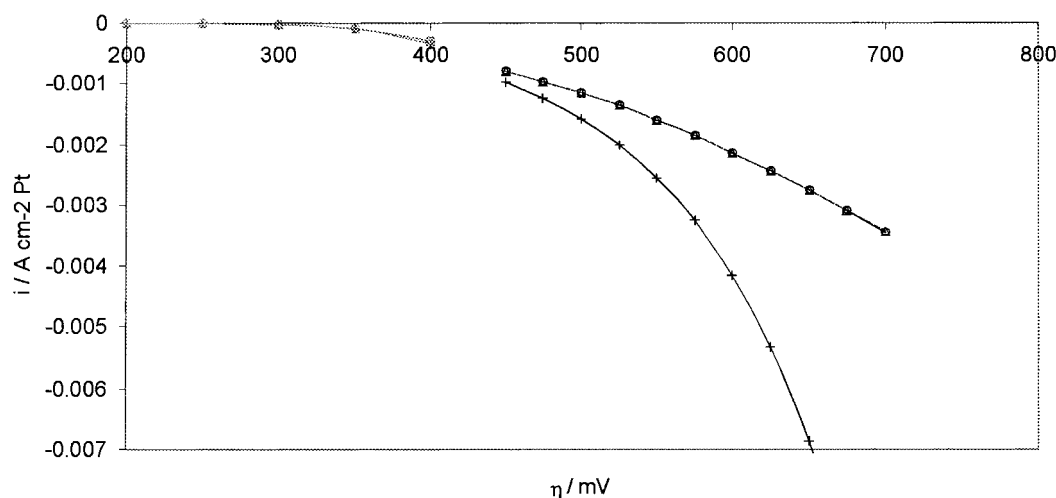

Fig. 4. Polarization curves for cathodic oxygen reduction predicted by the classical and modified models for a realistic active layer ($L = 10^{-5}$ m, $\gamma = 31.2$ m^2 m^{-2}, $DC_0 = 10^{-9}$ mol m^{-1} s^{-1}, $\kappa = 0.1$ S m). Classical model without ohmic drop limitation for low current densities ($i_o = 1 \times 10^{-6}$ A m^{-2}, $b = 0.060$ V decade^{-1}): ($\cdots + \cdots$) and for high current densities ($i_o = 1.4 \times 10^{-2}$ A m^{-2}, $b = 0.12$ V decade^{-1}): (— + —). Classical model with diffusion and ohmic drop, for low current densities: ($\cdots\bigcirc\cdots$) and for high current densities (— $\bigcirc$ —). Modified model with diffusion and ohmic drop, for low current densities: ($\cdots\bigstar\cdots$) and for high current densities (— $\bigstar$ —).
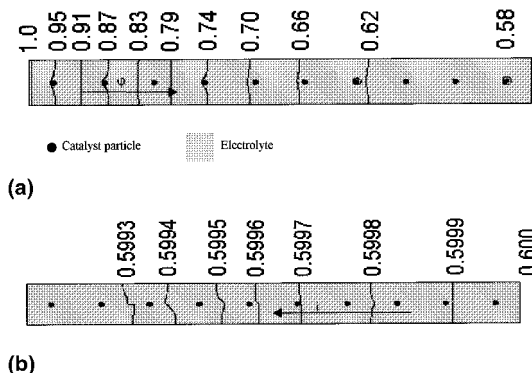
Fig. 5. Contour plots for concentration (a) and potential (b) in a thin active layer ($L = 10^{-6}$ m, $\gamma = 0.4$ m^{-2} m^{-2}) from the modified model for oxygen reduction at cathode ($U = 1.42 - u = 1.8 \times 10^{-2}$; $V = 4.6 \times 10^{-3} - 5.8 \times 10^{-5}$).
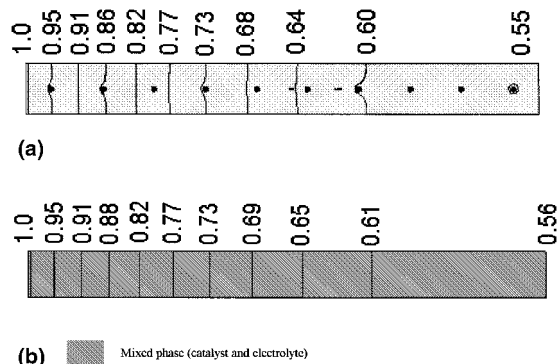

Fig. 6. Predicted contour plots for concentration in the active layer calculated from the modified (a) and classical (b) models for oxygen reduction at cathode neglecting ohmic drop limitation ($U = 1.4 - u = 1.8 \times 10^{-2}$). ($i_o = 1.4 \times 10^{-2}$ A m^{-2}, $b = 0.12$ V decade^{-1}, $|\eta_0| = 0.60$ V and $DC_0 = 10^{-9}$ mol m^{-1} s^{-1} and $\kappa = 1$ S m^{-1} at 353).

compared to diffusion for a large active layer as classically considered.

3.2. Anodic hydrogen oxidation: case of fast kinetics

For hydrogen oxidation, the classical model overestimates the current density in comparison to that predicted from the modified model (Figure 7). The results are significantly different and can be easily understood by studying the concentration and potential curves distribution within a thin active layer (Figure 8).

For hydrogen oxidation (Figure 8), the modified model also predicts a quasi-linear distribution for concentration over the whole active layer (Figure 8(a)). However, a deviation from the linear concentration profile can be observed close to the catalyst particles for fast kinetics. The concentration profile shows a planar flux density toward the electrolyte layer and a spherical flux density at the particle level with a strong local concentration gradient for catalyst particles located close to the gas–electrolyte interface. Figure 8(b) shows the potential distribution within the active layer predicted by the modified model. As previously, the

equipotential curves have a quasi-linear shape with a slight curvature close to the catalyst particles. As a conclusion, the discrete distribution of catalyst phase does not provides any significant modification in predicting the potential profiles for hydrogen oxidation ($v < 1$). In contrast it strongly acts on concentration profiles ($u \geqslant 1$).

In such a case, diffusion and ohmic drop limitations are no longer negligible at the particle level and the dimensionless parameter u becomes greater than unity while v is close to 1. Indeed the resulting current density, concentration and overpotential profiles for hydrogen oxidation predicted by the modified and classical models are significantly different (Figure 9). Comparison between the two models clearly shows that the hypothesis of uniform distribution of catalyst phase leads to an overestimated concentration gradient close to the gas–electrolyte interface and an optimistic catalyst utilisation rate [14, 16] (Figure 9).

Moreover, the concentration profiles are also very different according to whether ohmic drop (Figures 8(a) and 9(a)) is taken into account or not (Figures 10(a)
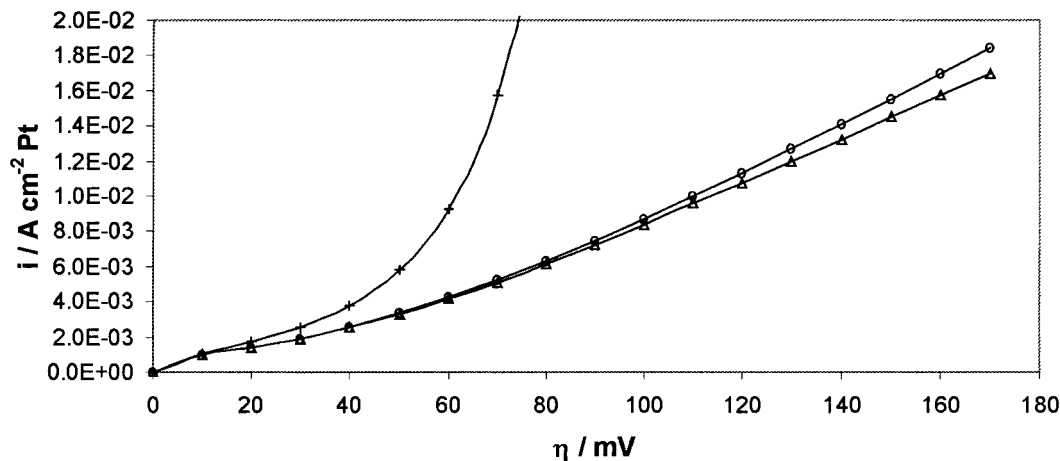

Fig. 7. Polarization curves for hydrogen oxidation ($i_o = 10^2$ A m^{-2}, $b = 0.030$ V decade^{-1}) predicted by the classical model without ohmic drop (— + —); the classical model with diffusion and ohmic drop (— ○ —) and the modified model with diffusion and ohmic drop (— ★ —); for an active layer ($L = 10^{-5}$ m, $\gamma = 31.2$ m^2 m^{-2}, $DC_0 = 10^{-9}$ mol m^{-1} s^{-1}, $\kappa = 1$ S m^{-1}).
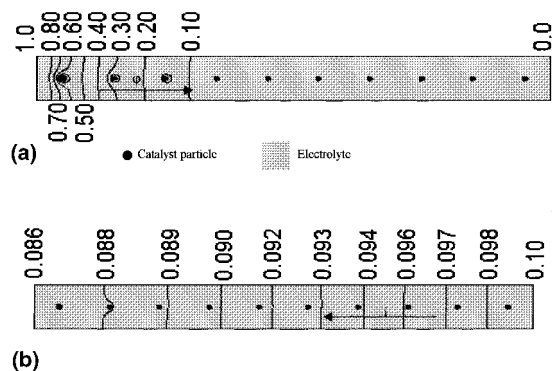
Fig. 8. Contour plots for concentration (a) and potential (b) in a thin active layer ($L = 10^{-6}$ m, $\gamma = 0.4$ m^{-2} m^{-2}) from the modified model for hydrogen oxidation at the anode ($U = 443 - u = 5.5$; $V = 28.5 - v = 0.35$). ($i_0 = 10^2$ A m^{-2}, $b = 0.030$ V decade^{-1}, $\eta_0 = 0.10$ V and $DC_0 = 10^{-9}$ mol m^{-1} s^{-1}, $\kappa = 0.1$ S m^{-1}).
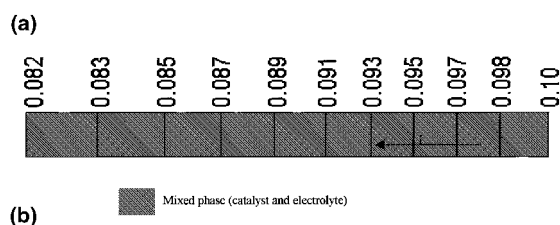
Fig. 9. Contour plots for concentration (a) and potential (b) in a thin active layer ($L = 10^{-6}$, $\gamma = 0.4$ m^{-2} m^{-2}) from the classical model for hydrogen oxidation at the anode ($U = 443 - V = 28.5$). ($i_0 = 10^2$ A m^{-2}, $b = 0.030$ V decade^{-1}, $\eta_0 = 0.10$ V and $DC_0 = 10^{-9}$ mol m^{-1} s^{-1}, $\kappa = 0.1$ S m^{-1}).

and (b)). In fact, ohmic drop resistances over the whole active layer, which are no longer negligible ($V \gg 1$), decrease the kinetic rate close to the gas–active layer interface. As a result, hydrogen is steadily consumed and concentration gradients are smaller than those predicted when only considering mass transfer limitations (Figure 9(a)). In such conditions, catalyst particles act in a more uniform way. Furthermore for a thicker active
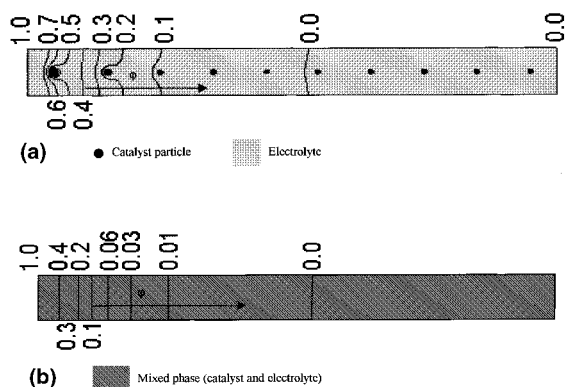
Fig. 10. Predicted contour plots for concentration in a thin active layer ($L = 10^{-6}$, $\gamma = 0.4$ m^{-2} m^{-2}) using the modified (a) and classical (b) models for hydrogen oxidation at anode neglecting ohmic drop ($U = 440 - u = 5.5$) ($i_0 = 10^2$ A m^{-2}, $b = 0.030$ V decade^{-1}, $\eta_0 = 0.10$ V and $DC_0 = 10^{-9}$ mol m^{-1} s^{-1}).

layer, ohmic drop induces a strong limitation at the level of the whole active layer thickness.

As a rule, the classical model is quite suitable in describing the working behaviour of the active layer for slow kinetics [11] when parameters u and v remain small compared to one. In contrast, the concentration and potential profiles are very different for fast kinetics (u and $v > 1$), depending on whether the discrete character of the catalyst phase distribution is taken into account. The classical model, which is generally used to describe the active layer working behaviour, is then not able to describe the actual electrode working and overestimates the performance of the PEMFC.

4. Conclusion

This work confirms that the discrete distribution of catalyst phase as isolated nanoparticles can play an important role on mass and charge transport in the active layers of a PEMFC. This influence results from spherical diffusion and ohmic drop close to the catalyst particles, which are able to strongly modify both the concentration and potential distributions and thus the predicted current densities. Moreover, this study demonstrates that the ohmic drop limitation cannot be neglected as classically assumed, at the level of the whole active layer thickness for high current densities, large active layer thickness or low ionic conductivity.

These limitations at the particle level appear to be insignificant in the case of oxygen reduction. In such conditions, the classical model remains suitable for describing the working behaviour of the cathode. In contrast, diffusion resistance at the particle level becomes predominant for hydrogen oxidation requiring the use of the modified model which is presented here.

Four dimensionless parameters are proposed to determine the limiting phenomenon within the active layer. These criteria allow selection of the more suitable model to describe both mass and charge transfer in the active layer: parameters U and V estimate the influence of transport resistance at the whole active layer level, while u and v are related to the transport resistances at the particle level. When parameters u and v tend to unity, the classical model is not able to describe the working behaviour of the active layer and the modified model must be used.

The present approach is not limited to fuel cell electrodes but may also be used with advantage to any anodic or cathodic reaction occurring in the active layer of porous electrodes using catalyst particles flooded with electrolyte.

References

1. S. Srinivasan, H.D. Hurwitz and J. O'M Bockris, *J. Chem. Phys.* **46** (1967) 3108.
2. S. Srinivasan and H.D. Hurwitz, *Electrochim. Acta* **12** (1967) 495.

3. J. Giner and C. Hunter, *J. Electrochem. Soc.* **116** (1969) 1124.
4. T.E. Springer, T.A. Zawodzinski and S. Gottesfeld, *J. Electrochem. Soc.* **138** (1991) 2334.
5. T.F. Fuller and J. Newman, *J. Electrochem. Soc.* **140** (1993) 1218.
6. D.M. Bernardi and M.W. Verbrugge, *J. Electrochem. Soc.* **139** (1992) 2477.
7. T.E. Springer, M.S. Wilson and S. Gottesfeld, *J. Electrochem. Soc.* **140** (1993) 3513.
8. M.L. Pery, J. Newman and E.J. Cairns, *J. Electrochem. Soc.* **145** (1998) 5.
9. J. Perez, A.A. Tanaka, E.R. Gonzales and E.A. Ticianelli, *J. Electrochem. Soc.* **141** (1994) 1070.
10. F. Gloaguen, F. Andolfatto, R. Durand and P. Ozil, *J. Appl. Electrochem.* **24** (1994) 863.
11. O. Antoine, Y. Bultel, R. Durand and P. Ozil, *Electrochim. Acta* **43** (1998) 3681.
12. Y. Bultel, R. Durand and P. Ozil, *Electrochim. Acta* **43** (1998) 1077.
13. Y. Bultel, R. Durand and P. Ozil, *AIDIC Conferences Series*, **2** (1997) 405.
14. Y. Bultel, P. Ozil, R. Durand and D. Simonsson, in S. Gottesfeld, G. Halpert and A. Landgrebe (Eds), 'Proton Conducting Membrane Fuel Cells', **PV. 95-23** Proceedings series (The Electrochemical Society, Pennington, NJ, 1995), p. 34.
15. Y. Bultel, P. Ozil and R. Durand, *J. Appl. Electrochem.* **28** (1998) 269.
16. Y. Bultel, P. Ozil and R. Durand, *J. Appl. Electrochem.* **29** (1999) 1025.
17. A. Parthasarathhy, S. Srinivasan, A.J. Appleby and C.R. Martin, *J. Electrochem. Soc.* **139** (1992) 2530.
18. R.M.Q. Mello and E.A. Ticianelli, *Electrochim. Acta* **42** (1997) 1031.
19. J.J. Summer, S.E. Creager, J.J. Ma and D. DesMarteau, *J. Electrochem. Soc.* **145** (1998) 107.
20. J.M. Ortega and W.C. Rheinboldt, 'Iterative Solution of Nonlinear Equations in Several Variables' (Academic Press, New York, 1970).
21. M. Watanabe, H. Sei and P. Stonehart, *J. Electroanal. Chem.* **261** (1981) 375.
22. P. Stonehart and P. Ross, *Electrochim. Acta* **21** (1976) 441.

Appendix

In this Appendix, the process leading to the specific the finite element equation is presented in order to numerically solved the physical problem. Equations 10 and 11 are solved in a domain (Ω) with the boundary conditions (6, 7 and 12) imposed at the interface ($\partial\Omega$).

Using a projective function α, Laplace equations (10 and 11) can be transformed to the integral equation:

$$\iint_{\Omega} \alpha \nabla \cdot (-\sigma \nabla \Phi) \mathrm{d}S = 0 \qquad (A1)$$

Since for any scalar p and vector A:

$$\nabla(pA) = p\nabla A + A\nabla p \qquad (A2)$$

Equation 1 may be written as

$$\iint_{\Omega} \alpha \nabla \cdot (-\sigma \nabla \Phi) \mathrm{d}S = \iint_{\Omega} \nabla \cdot (-\alpha \sigma \nabla \Phi) \mathrm{d}S$$
$$+ \iint_{\Omega} \sigma(\nabla \Phi \nabla \alpha) \mathrm{d}S \qquad (A3)$$

The Green–Ostogradski theorem leads to $\iint_{\Omega} \nabla(A)\mathrm{d}S = \int_{\partial\Omega}(A)n\,\mathrm{d}l$. Then,

$$\iint_{\Omega} \nabla \cdot (-\alpha \sigma \nabla \Phi) \mathrm{d}S = \int_{\partial\Omega} (-\alpha \sigma \nabla \Phi) n\,\mathrm{d}l \qquad (A4)$$

where n is the normal vector.

The boundary condition can thus be introduced by replacing the divergence term (Equation 4) by the charge transfer kinetic term (Equation 12) at the electrolyte–nanoparticle interface (nonhomogeneous Neumann condition):

$$\int_{\partial\Omega} (-\alpha D \nabla C) n\,\mathrm{d}l = \int_{\partial\Omega} \alpha \frac{i_{\mathrm{o}}}{nF} \exp\left(\frac{2.3\,\eta}{b}\right) \frac{C}{C_0}\,\mathrm{d}l \qquad (A5)$$

$$\int_{\partial\Omega} (-\alpha \kappa \nabla \eta) n\,\mathrm{d}l = \int_{\partial\Omega} \alpha i_{\mathrm{o}} \exp\left(\frac{2.3\,\eta}{b}\right) \frac{C}{C_0}\,\mathrm{d}l \qquad (A6)$$

Taking into account the boundary conditions, the final soft coupled equations between the concentration and the overpotential are expressed as

$$\iint_{\Omega} D\nabla\alpha\nabla C\,\mathrm{d}S = \int_{\partial\Omega} \alpha \frac{i_{\mathrm{o}}}{nF} \exp\left(\frac{2.3\,\eta}{b}\right) \frac{C}{C_0}\,\mathrm{d}l \qquad (A7)$$

$$\iint_{\Omega} \kappa\nabla\alpha\nabla\eta\,\mathrm{d}S = \int_{\partial\Omega} \alpha i_{\mathrm{o}} \exp\left(\frac{2.3\,\eta}{b}\right) \frac{C}{C_0}\,\mathrm{d}l \qquad (A8)$$

In the Galerkin formulation, C and η are approximated in each finite element using the Lagrange polynomial function α_j and the values of the unknowns C_j and η_j at each node j. Using this approximation, Equations 7 and 8 are transformed into matrix systems which are solved.